Purdue University

Purdue e-Pubs

Other Nanotechnology Publications

Birck Nanotechnology Center

1-25-2005

Effect of electron-nuclear spin interactions for electron-spin qubits localized in InGaAs self-assembled quantum dots

Seungwon Lee
Jet Propulsion Laboratory

Paul von Allmen
Jet Propulsion Laboratory

Fabiano Oyafuso
Jet Propulsin Laboratory

Gerhard Klimeck
Purdue University - Main Campus, gekco@purdue.edu

Follow this and additional works at: http://docs.lib.purdue.edu/nanodocs

Effect of electron-nuclear spin interactions for electron-spin qubits localized in InGaAs self-assembled quantum dots

Seungwon Lee,[a] Paul von Allmen, Fabiano Oyafuso, and Gerhard Klimeck
Jet Propulsion Laboratory, California Institute of Technology, Pasadena, California 91109

K. Birgitta Whaley
Department of Chemistry, University of California, Berkeley, California 94720

The effect of electron-nuclear spin interactions on qubit operations is investigated for a qubit represented by the spin of an electron localized in an InGaAs self-assembled quantum dot. The localized electron wave function is evaluated within the atomistic tight-binding model. The electron Zeeman splitting induced by the electron-nuclear spin interaction is estimated in the presence of an inhomogeneous environment characterized by a random nuclear spin configuration, by the dot-size distribution, alloy disorder, and interface disorder. Due to these inhomogeneities, the electron Zeeman splitting varies from one qubit to another by the order of 10^{-6}, 10^{-6}, 10^{-7}, and 10^{-9} eV, respectively. Such fluctuations cause errors in exchange operations due to the inequality of the Zeeman splitting between two qubits. However, the error can be made lower than the quantum error threshold if an exchange energy larger than 10^{-4} eV is used for the operation. This result shows that the electron-nuclear spin interaction does not hinder quantum-dot based quantum computer architectures from being scalable even in the presence of inhomogeneous environments. © *2005 American Institute of Physics.* [DOI: 10.1063/1.1850605]

I. INTRODUCTION

Quantum computers (QC) hold the promise of solving problems that would otherwise be beyond the practical range of conventional computers.[1] Natural candidates for the fundamental building block of quantum computers (qubit) are the electronic and the nuclear spins, since they have a well defined Hilbert space and a relatively long decoherence time compared to the orbital degrees of freedom. Several QC implementations have been proposed based on the use of the spin degree of freedom, such as using the nuclear spins in a molecule[2] and in crystal lattices,[3] the nuclear spins of donors in Si[4] and in endohedral fullerenes,[5] and the spin of electrons confined in quantum dots[6,7] or donors.[8] While small-scale quantum computing has been demonstrated with a few qubits using the nuclear spin[9–11] or trapped ions,[12] large-scale quantum computing with many qubits used in parallel is yet to be demonstrated.

Solid-state spin-based QC architectures are in principle scalable to many qubits. However, they are intrinsically inhomogeneous due to defects, impurities, alloys, interfaces, strain, etc. Although the inhomogeneous environment will cause inaccuracy in the qubit operations, fault-tolerant error-correction schemes have been shown to compensate for errors up to a certain threshold.[13–16] For spin-based QC architectures, the single-qubit operation typically uses the Zeeman coupling to an external magnetic field ($g\mu_B \mathbf{S} \cdot \mathbf{B}$), while the two-qubit operation relies on the exchange interaction between two spins ($J\mathbf{S}_1 \cdot \mathbf{S}_2$). In these operations, if the inhomogeneous environment causes fluctuations in the Zeeman energy E_Z, it will lead to operational errors. For example, a

recent study[17] has shown that a "swap" operation with a Zeeman energy fluctuation ΔE_Z yields an error of $(\Delta E_Z/J)^2$. It is thus crucial to examine whether the proposed solid-state spin-based QC implementations are scalable within the quantum error limit, in presence of a realistic inhomogeneous environment. As a prototype of this examination, the present paper focuses on the scalability of architectures where the qubit is represented by an excess electron spin localized in an InGaAs self-assembled quantum dot. An array of InGaAs self-assembled quantum dots is an excellent candidate for a scalable QC architecture because recent advances in the fabrication technology have substantially improved the control of size and location of the nanostructures.[18–24]

The electron Zeeman energies of InGaAs self-assembled quantum dots can fluctuate due to inhomogeneous hyperfine energies induced by the electron-nuclear spin interaction. This fluctuation of the hyperfine energies can be quite large since all the nuclei in an InGaAs quantum dot and its environment GaAs buffer have nonzero magnetic moment and the resulting number N of nuclei interacting with the electron spin is in the range $10^4–10^6$. The hyperfine energy generated by such a large number of nuclear spins varies from dot to dot, due to the various sources of the inhomogeneous environment. A recent study showed that when the nuclei are unpolarized, the fluctuation of the hyperfine energies due to the random nuclear spin distribution is proportional to $1/\sqrt{N}$ and is as large as $10^{-7}–10^{-6}$ eV for $N=10^4–10^6$.[25] The fluctuation can be suppressed by polarizing the nuclear spins using dynamic polarization schemes.[26–30] However, the fluctuation of the hyperfine energies is persistent even in polarized nuclei because of other sources of inhomogeneity in the environment. For example, the dot-size distribution, alloy disorder, and interface disorder are inherent to self-

---
[a] Electronic mail: seungwon.lee@jpl.nasa.gov

assembled quantum dots. We find here that the electron-nuclear spin interaction in an inhomogeneous environment can lead to a fluctuation of the hyperfine energies as large as that due to the random nuclear distribution in the case of unpolarized nuclei.

In addition to the inhomogeneous hyperfine energies, fluctuation in the electron Zeeman energies can arise from the fluctuation of the electron Landé factor g and the fluctuation of the local magnetic field due to, e.g., magnetic impurities. In particular, considerable fluctuations of the electron g factor are expected due to the inhomogeneous dot size, strain, and alloy disorder.[31–33] Moreover, the electron g factor can be artificially fluctuated (i.e., engineered) by an external electric and magnetic field.[34–36] The estimation of the g-factor fluctuation due to these sources is reserved for future work.

The electron-nuclear spin interaction in III–V material quantum dots has been intensively studied over the last few years.[25,37–44] The focus of these studies has been to understand the effect of the interaction on electron spin relaxation, ensemble spin dephasing, and spin decoherence. These investigations have shown that the electron-nuclear spin interaction is one of the dominant mechanisms for electron spin relaxation and decoherence, prevailing over the mechanism related to spin-orbit coupling under certain circumstances.[41] In clear distinction from these previous investigations, the focus of the present work is to estimate the fluctuations of the electron hyperfine energies in the presence of an inhomogeneous environment and to investigate its consequence for quantum gate operations. Furthermore, most of the previous work has concentrated on gate-controlled GaAs quantum dots in GaAs–AlGaAs heterostructures,[45,46] where the lateral confinement is much weaker than the vertical confinement. In contrast, a self-assembled quantum dot, the subject of the present work, is strongly confined in both lateral and vertical directions. Due to the stronger lateral confinement, the self-assembled quantum dot has a larger energy spacing between confined levels, which is typically about 10–100 meV in contrast to about 1 meV for gate-controlled GaAs quantum dots.

In this paper, we first estimate the fluctuations in the hyperfine energies resulting from the electron-nuclear spin interaction in the presence of inhomogeneities in the environments,—in particular dot-size distribution, alloy disorder, and interface disorder. We calculate the electron density using the atomistic $sp^3d^5s^*$ tight-binding model. The tight-binding model is ideally suited for the description of alloy and interface disorder with atomistic resolution, which enables us to study the microscopic effect of the inhomogeneous environment on the electron densities. In the second stage, we evaluate the effect of the resulting fluctuations in the electron hyperfine energies on qubit operations.

The paper is organized as follows. Section II describes the treatment of the electron-nuclear spin interaction within the tight-binding model. Section III describes the fluctuation of the hyperfine energies of the electron spin from one quantum dot to another due to the inhomogeneous environment.

Section IV discusses the effect of the fluctuation of the hyperfine energies on qubit operations. Finally, Sec. V summarizes the results of this work.

II. ELECTRON-NUCLEAR SPIN INTERACTION

The electron-nuclear spin interaction originates from the coupling of the nuclear magnetic moment to the magnetic field generated by the electron magnetic moment (or equivalently from the coupling of the electron magnetic moment to the magnetic field generated by the nuclear magnetic moment). Both the spin and orbital angular momentum of the electron contribute to its magnetic moment. Therefore, the electron-nuclear spin interactions for an electron in an s-symmetry orbital and in a non-s-symmetry orbital are expressed as follows:[47]

$$H_{HF} = \frac{16\pi}{3}\gamma_I\mu_B\mu_N\delta(\mathbf{r})[\mathbf{S}\cdot\mathbf{I}], \quad l = 0 \tag{1}$$

$$H_{HF} = \frac{2\gamma_I\mu_B\mu_N}{r^3}\left[(\mathbf{L}-\mathbf{S})\cdot\mathbf{I} + 3\frac{(\mathbf{S}\cdot\mathbf{r})(\mathbf{I}\cdot\mathbf{r})}{r^2}\right], \quad l \neq 0. \tag{2}$$

Here, γ_I, μ_B, and μ_N are the gyro-magnetic factor of the nuclear spin, the Bohr magneton, and the nuclear magneton, respectively. $\mathbf{S}$ and $\mathbf{I}$ are the spin operators for the electron and the nucleus, and $\mathbf{L}$ is the angular momentum operator for the electron. When hydrogen-like atomic orbitals are considered, the first-order energy shifts due to the electron-nuclear spin interaction for both s-symmetry and non-s-symmetry electron orbitals are comparable.[47]

The conduction electron wave function in an InGaAs self-assembled dot is mostly composed of s-symmetry atomic orbitals, as shown in Table I. For the lowest electron wave function in InAs quantum dots, the tight-binding calculation shows that the contribution of s and s^* orbitals is about 94%, while the contributions of p and d orbitals are about 5% and 1%, respectively. This small admixture can be understood from the wave function symmetry in bulk. While there is no admixture at Γ_{6c}, Table I shows that the contributions from p and d orbitals increase for wave vectors away from the center of the Brillouin zone. The same trend is reported in psudopotential studies and another tight-binding calculation.[48–50] The effective wave vector of the electron wave function in the quantum dot is roughly $(\pi/L_x, \pi/L_y, \pi/L_z)$ where L_x, L_y, and L_z are the dot dimensions. The wave vector is not at Γ although it is close to Γ. Therefore, the small p and d orbital admixture in the quantum-dot wave function originates from the bulk wave function symmetry at a wave vector that is not at Γ.

The effective electron magnetic field generated by each electron orbital is roughly proportional to its weight in the wave function. This means that the contribution of p and d orbitals to the effective magnetic field is about 6%. Since we are interested in the order of magnitude of the hyperfine energy (and its fluctuation), we therefore choose to ignore the electron-nuclear spin interaction due to a non-s-symmetry orbital. As a result, the remaining electron-nuclear spin interaction is described by the hyperfine Fermi contact term:

TABLE I. Projection of the lowest electron wave function onto the atomic orbitals of different symmetry for lens-shaped InGaAs quantum dots (QD) with diameter 15 nm and height 6 nm. The wave function is calculated with an $sp^3d^5s^*$ tight-binding model. Three different alloy materials are considered for quantum dots. For comparison, the wave functions of the lowest conduction band at Γ and X in bulk InAs and GaAs are also projected onto the atomic orbitals.

Material	s symmetry		p symmetry	d symmetry
	s	s^*	p	d
InAs QD	0.738	0.195	0.051	0.015
$In_{0.8}Ga_{0.2}As$ QD	0.762	0.184	0.042	0.012
$In_{0.6}Ga_{0.4}As$ QD	0.783	0.174	0.023	0.010
InAs Bulk at Γ_{6c}	0.827	0.173	0.000	0.000
GaAs Bulk at Γ_{6c}	0.844	0.156	0.000	0.000
InAs Bulk at X_{6c}	0.204	0.001	0.337	0.457
GaAs Bulk at X_{6c}	0.055	0.019	0.434	0.492

$$\mathbf{H}_{HF} = \frac{16\pi}{3}\mu_B\mu_N\sum_j \gamma_j(\mathbf{S}\cdot\mathbf{I_j})\delta(\mathbf{r}-\mathbf{R_j}), \qquad (3)$$

where γ_j and $\mathbf{I}_j$ are the gyro-magnetic factor and the spin operator of the jth nucleus. $\mathbf{r}$ and $\mathbf{R}_j$ are the position vectors for the electron and the jth nucleus. Since the energy of the hyperfine interaction (<0.1 meV) is much smaller than the energy spacing between the quantized electron levels (about 10–100 meV), the hyperfine Hamiltonian for a given electron level can be approximated with first-order perturbation theory as:

$$\mathbf{H}_{HF} = \frac{16\pi}{3}\mu_B\mu_N\sum_j \gamma_j|\psi(\mathbf{R}_j)|^2(\mathbf{S}\cdot\mathbf{I}_j)=\sum_j A_j(\mathbf{S}\cdot\mathbf{I}_j), \quad (4)$$

where $\psi(\mathbf{R}_j)$ is the electron wave function at nuclear site $\mathbf{R}_j$, and A_j is the effective hyperfine coupling constant between the electron and the jth nuclear spin.

The coupling constant A_j is proportional to the square of the electron wave function at the nuclear site $\mathbf{R}_j$

$$A_j = \frac{16\pi}{3}\mu_B\mu_N\gamma_j|\psi(\mathbf{R_j})|^2. \qquad (5)$$

Within the tight-binding model, the electron wave function is expressed as a linear combination of atomic basis orbitals $\phi(\mathbf{r}-\mathbf{R}_j)$. The present tight-binding model includes $sp^3d^5s^*$ basis orbitals.[51] Therefore, the total electron density at nuclear site $\mathbf{R}_j$ is given by s-symmetry orbital densities:

$$|\psi(\mathbf{R}_j)|^2 = |\alpha_j\phi_s(0) + \beta_j\phi_{s^*}(0)|^2, \qquad (6)$$

where α_j and β_j are the tight-binding coefficients for s and s^* orbitals centered at site $\mathbf{R}_j$, respectively. In terms of the effective mass approximation, the tight-binding coefficients loosely speaking correspond to the envelope functions while the tight-binding orbitals correspond to the Bloch wave functions.

The tight-binding coefficients α_j and β_j depend on dot geometry, material, strain profile, alloy disorder, etc. The geometry of a quantum dot grown by molecular beam epitaxy varies widely with the growth condition.[52–54] Based on the experimentally achievable geometries, we model a lens-shaped self-assembled InAs dot with diameter 15 nm and height 6 nm, as shown in Fig. 1. Since the dots are embedded in a GaAs matrix, InAs–GaAs self-assembled dots are strongly strained due to the large lattice mismatch of 7% between InAs and GaAs. The equilibrium atomic positions under strain are calculated with an atomistic valence force field model.[55] Following the strain calculation, the electron wave function in the strained nanostructure is obtained with the empirical $sp^3d^5s^*$ tight-binding model including the spin-orbit coupling.[51] The strain effect on the electronic structure is captured by adjusting the atomic energies of the tight-binding model with a linear correction that is obtained within the Löwdin orthogonalization procedure.[51,56] We also modify the nearest-neighbor coupling parameters for the strained structures according to the generalized version of Harrison's d^2 scaling law and the Slater–Koster direction-cosine rule.[57,58]

In the empirical tight-binding model, $\phi_s(0)$ and $\phi_{s^*}(0)$ are unknown because the model determines the Hamiltonian matrix elements without introducing the real-space description of the basis orbitals. For this work, the densities of the basis orbitals at a nuclear site are determined empirically using measurements of the Overhauser shift of the electron spin resonance.[59] The details of determining the densities are given in the Appendix.

With the resulting α_j, β_j, $\psi_s(0)$, and $\psi_{s^*}(0)$, A_j is calculated according to Eqs. (5) and (6). The spatial distributions of A_j along the directions of the dot diameter and dot height are plotted in Fig. 2. The maximum value of $A_j(7$ neV) is found at the As nucleus located at the center of the quantum dot. The A_j value associated with an As nucleus is about 1.7 times larger than that associated with the In and Ga nuclei.
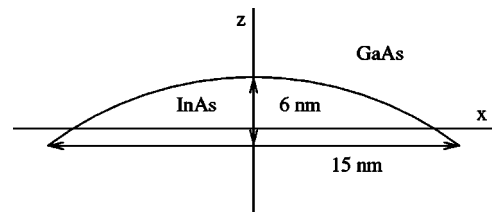

FIG. 1. Geometry of the modeled self-assembled quantum dot. The quantum dot is lens shaped with a base diameter of 15 nm and a height of 6 nm. The lines x and z are the transverse and vertical axes along which the spatial distributions of A_j are plotted in Fig. 2.
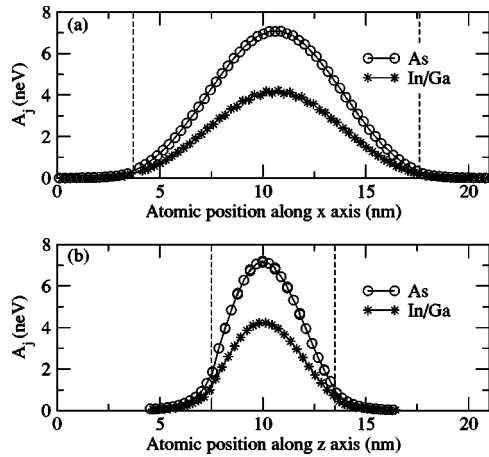
FIG. 2. Spatial distributions of the hyperfine coupling coefficient (A_j) for a lens-shaped InAs quantum dot embedded in a GaAs buffer (a) along the x axis and (b) along the z axis of Fig. 1. The coupling coefficient A_j is given by Eq. (5) and is proportional to the electron density. The dashed lines indicate the interface between the InAs dot and the GaAs buffer.

This large difference is due to the larger electron density on anions than on cations. The global distribution of A_j reflects the localization of the electron density inside the dot. Although the electron confinement inside the dot is quite effective along the lateral direction, along the vertical axis the electron density extends farther outside the dot. This causes the electron spin to interact with a large number of nuclei outside the dot, in addition to the interaction with the nuclei inside the dot. The number of nuclei for which A_j is larger than $0.01 * \max(A_j)$ is about 60 000, whereas the number of nuclei inside the dot is about 30 000.

III. FLUCTUATION OF THE HYPERFINE SPLITTING

A typical quantum-computer architecture involves an external magnetic filed $B\hat{z}$ to define the qubit space. The spin up and spin down states of the electron in the external magnetic field $B\hat{z}$ are split by $g\mu_B B$. The two levels are further split by the electron-nuclear spin interaction. According to Eq. (4), the hyperfine splitting is given by

$$E_{\mathrm{HF}} = E_\uparrow - E_\downarrow = \sum_j A_j I_j^z, \qquad (7)$$

where I_j^z is the expectation value of operator $\hat{I}_j^z$ over the nuclear spin states. The hyperfine splitting is determined by the spatial distributions of both A_j and I_j^z. Hence, if A_j and I_j^z vary from dot to dot, the hyperfine splitting fluctuates as well. The variations of A_j and I_j^z arise from inhomogeneity in the environment, such as the nuclear spin orientation, the dot-size distribution, the alloy and interface disorder.

To estimate the fluctuation of the hyperfine splitting, we take the following approach. First, the hyperfine splitting fluctuation is estimated for one inhomogeneity source at a time while other inhomogeneity sources are assumed to be eliminated. Second, the inhomogeneity source is treated as a random source since the correlation among quantum dots for each of the inhomogeneity sources is negligible. Third, the effect of the inhomogeneity source on the electron wave function (i.e., A_j) is examined. If the effect is negligible, the

electron wave function is assumed to be unchanged. Otherwise, the electron wave function is recalculated for several configurations of the dot environment.

We first consider the hyperfine splitting fluctuation due to the nuclear spin orientation. When the nuclear spins are unpolarized, the nuclear spins in the magnetic field at thermal equilibrium are distributed among the eigenstates of $\hat{I}_j^z$ with a probability proportional to the Boltzmann factor $\exp(\gamma_j \mu_N I_j^z B / k_B T)$. Since the thermal energy $k_B T$ is typically much larger than the nuclear Zeeman energy $\gamma_j \mu_N I_j^z B$, it is safe to assume that the nuclear spins are randomly distributed among the eigenstates of $\hat{I}_j^z$ with a uniform probability distribution. It is also reasonable to assume that the random nuclear spin orientation does not change the electron wave function and thus the coupling constant A_j, because the electron-nuclear spin interaction is much smaller than the electron-nuclear charge interaction. Taking into account the above reasoning, the fluctuation of the hyperfine splitting due to the random nuclear spin orientations is given by

$$\begin{aligned}
\Delta E_{\mathrm{HF}} &= \sqrt{\langle E_{\mathrm{HF}}^2 \rangle_{\mathrm{ens}} - \langle E_{\mathrm{HF}} \rangle_{\mathrm{ens}}^2} \\
&= \sqrt{\sum_j \left[A_j^2 \langle (I_j^z)^2 \rangle_{\mathrm{ens}} - A_j^2 \langle I_j^z \rangle_{\mathrm{ens}}^2 \right]} \\
&= \sqrt{\sum_j A_j^2 I_j (I_j + 1)/3}, \qquad (8)
\end{aligned}$$

where $\langle \cdots \rangle_{\mathrm{ens}}$ is an average over the ensemble of dots. Note that the fluctuation is only due to the random nuclear spin orientation while other inhomogeneity sources are suppressed; the dot geometry and atomic configuration in the alloy and near the interface are identical for all the dots. Due to the random distribution of the nuclear spin within the ensemble, $\langle I_j^z \rangle_{\mathrm{ens}}$ is zero and $\langle (I_j^z)^2 \rangle_{\mathrm{ens}}$ is $I_j(I_j+1)/3$ for all j. Furthermore, the nuclear spins are assumed to be uncorrelated, i.e., $\langle I_j^z I_k^z \rangle_{\mathrm{ens}} = \langle I_j^z \rangle_{\mathrm{ens}} \langle I_k^z \rangle_{\mathrm{ens}}$ for $j \neq k$.

The fluctuation ΔE_{HF} due to the random distribution of nuclear spins can be suppressed by polarizing the nuclear spins. The polarization can be achieved via the electron-nuclear spin interaction using spin-polarized current or optical pumping.[27–30,60,61] However, even when the nuclear spins are fully polarized, E_{HF} can still be broadened by other sources of inhomogeneity in the dot array. For example, an ensemble of self-assembled quantum dots has typically about a 10% size distribution, which is inherent to the nonequilibrium growth process of the molecular beam epitaxy.[62] As the dot size changes, the effective number of nuclei interacting with the confined electron and the spatial distribution of A_j change. This leads to different hyperfine splittings for dots with different sizes. The fluctuation in E_{HF} due to the size distribution will be estimated here by comparing calculated values of E_{HF} for three different dot geometries with base diameter and height values of (14 nm, 5.5 nm), (15 nm, 6 nm), and (16 nm, 6.5 nm), respectively. From the smallest to the largest dot, the number of nuclei inside the dot increases from 22 304 to 35 161.

We further consider two additional sources for the broadening of E_{HF} in self-assembled dots: Alloy and interface disorder. The alloy disorder stems from the fact that a

large number of atomic configurations will yield the same compositional ratio in an InGaAs quantum dot. The interfaces between an unalloyed InAs dot and the GaAs buffer is affected by In–Ga intermixing over a length scale of 1.25 nm, which is the origin of interface disorder.[63] When thermal annealing is applied after the growth of an InAs dot in order to tune its electronic structure, the In–Ga intermixing length becomes even larger.[64] The alloy and interface disorder lead to the broadening of E_{HF} in two ways. First, In and Ga have different nuclear spin quantum numbers ($I_{In}=9/2$, $I_{Ga}=3/2$). Second, they have different ionic potentials that will lead to a change in the electron densities (or A_j).

When the nuclear spins are polarized and the dot size is uniform, the fluctuation ΔE_{HF} due to the alloy and interface disorder is given by

$$\Delta E_{HF} = \sqrt{\sum_j \Delta^2(A_j I_j^z)}, \qquad (9)$$

where $\Delta^2(A_j I_j^z)$ is the variance of $A_j I_j^z$. The variance $\Delta^2(A_j I_j^z)$ is studied by examining three different atomic configurations for an $In_{1-x}Ga_x As$ dot. The three atomic configurations are constructed by randomly choosing the cation atoms as In or Ga with probability $1-x$ and x, respectively. The overlap between the wave functions for two arbitrary configurations is about 0.997, indicating that the fluctuation of the energy density (or A_j) is very small. Furthermore, the average of the density fluctuation per site is only about $10^{-4}\%$ of the average density. Therefore, we may justifiably choose to ignore the fluctuation of A_j and approximate ΔE_{HF} as

$$\Delta E_{HF} \approx \sqrt{\sum_j A_j^2 \Delta^2 I_j^z}. \qquad (10)$$

For the case of the alloy disorder in $In_{1-x}Ga_x As$ dots, $\Delta^2 I_j^z$ is calculated to be $x(1-x)(I_{In}-I_{Ga})^2$ for all In and Ga atoms and is zero for all As atoms. For the case of the interface disorder in InAs dots, $\Delta^2 I_j^z$ is $0.25(I_{In}-I_{Ga})^2$ for the In and Ga atoms in the interface region and is zero for all other atoms. Each cation atom site in the interface is taken to have probability 0.5 to be occupied by either an In or a Ga atom.

After calculating the fluctuation of E_{HF} due to the inhomogeneities in the environment as described above, we have obtained the following results. When the nuclear spins are unpolarized, a random nuclear spin configuration yields ΔE_{HF} on the order of 10^{-6} eV. When the nuclear spins are polarized, a 10% distribution of dot sizes also yields ΔE_{HF} of the order of 10^{-6} eV. When the nuclear spins are polarized and the dot size is uniform, the alloy disorder results in fluctuations on the order of 10^{-7} eV, while the interface disorder gives rise to fluctuations of the order of 10^{-9} eV. These results indicate that an unpolarized nuclear spin configuration and quantum dot size fluctuation are the dominant sources of the inhomogeneous hyperfine splitting. Since the electron localized in each quantum dot has a different hyperfine splitting, this leads to an ensemble dephasing characterized by a dephasing time $T_2^*=\hbar/\Delta E_{HF}$. The fluctuation of E_{HF} can be also seen as the fluctuation of the effective nuclear magnetic field $B_N=E_{HF}/g_e\mu_B$. The values of ΔE, T_2^*, and ΔB_N resulting from the inhomogeneous environments studied here are summarized in Table II.

TABLE II. Hyperfine-splitting fluctuation (ΔE_{HF}), ensemble-spin dephasing time ($T_2^*=\hbar/\Delta E_{HF}$), and effective nuclear magnetic field fluctuation ($\Delta B_N=\Delta E_{HF}/g_e\mu_B$) caused by various inhomogeneities for an InGaAs quantum dot embedded in a GaAs buffer. For unpolarized nuclei, each nuclear spin direction is chosen randomly. For dot-size fluctuations, the base diameter is set to 15 ± 1 nm and the height to 6 ± 0.5 nm. For alloy disorder, $In_{0.5}Ga_{0.5}As$ dots are examined and each cation atom is randomly chosen to be an In or a Ga atom. For interface disorder, each cation within a 1.25 nm thick interface between the dot and the buffer is randomly chosen to be an In or a Ga atom, reflecting the experimental observation of In–Ga mixing near the interface (Ref. 63).

Inhomogeneity	ΔE_{HF}(eV)	T_2^*(s)	ΔB_N(G)
Unpolarized nuclei	10^{-6}	10^{-10}	100
Dot-size fluctuation	10^{-6}	10^{-10}	100
Alloy disorder	10^{-7}	10^{-9}	10
Interface disorder	10^{-9}	10^{-7}	0.1

IV. EFFECT OF ELECTRON-NUCLEAR SPIN INTERACTION ON QUBIT OPERATIONS

First, we examine the effect of the electron-nuclear spin interaction on a two-qubit operation. As shown in Sec. III, the electron-nuclear spin interaction in the presence of the inhomogeneous environment leads to the fluctuation of the hyperfine splitting E_{HF} from qubit to qubit. Consequently, the fluctuation of E_{HF} causes the Zeeman energy to be different in the two qubits. When a two-qubit operation such as a "swap" operation uses the exchange interaction $J\mathbf{S}_1 \cdot \mathbf{S}_2$, the Zeeman-energy difference ΔE_Z between two qubits causes an error probability $\sim(\Delta E_Z/J)^2$.[17] It has been shown that in principle this swap error can be fixed by additional, subsequent exchange gate operations if ΔE_Z is known and stable.[65] However, the new pulse sequence adds complexities to swap operation, and the fidelity of the complex swap operation is sensitive to the pulse rise–fall times.[65] Therefore, we concentrate on the original swap operation and its swap error due to the Zeeman-energy difference.

A quantum error up to a certain threshold can be fixed by a fault-tolerant error correction code. The error threshold varies widely depending on the code and the assumption about the system and the error type.[66] For our analysis, we choose a conservative estimation of the error threshold 10^{-4}.[66,67] This threshold is obtained under the assumption that the constant process of error correction takes place after every logical gate. We note that the error threshold here is for the "probability" of getting the output orthogonal to the correct output, rather than for the "amplitude" of the output orthogonal to the correct one.

For the error correction codes to be able to repair errors in the swap operation, we require $(\Delta E_Z/J)^2 < 10^{-4}$. The Zeeman-energy fluctuation ΔE_Z due to the four different sources of inhomogeneity considered in this paper ranges from 10^{-9} to 10^{-6} eV. Hence, the exchange energy J should be larger than 10^{-4} eV. At the same time, to prevent the electron from being excited to higher-lying orbitals, J should be smaller than the electron energy spacing (ΔE_e) between the ground and the excited orbital. The excitation probability due to the exchange interaction is roughly on the order of

$(J/\Delta E_e)^2$. Therefore, a ratio $J/\Delta E_e < 10^{-2}$ would ensure that the electron stays in the qubit space with leakage probability below 10^{-4}.

The dual condition $(\Delta E_z \ll J \ll \Delta E_e)$ can be met with vertically stacked self-assembled dots.[68] A recent calculation with harmonic double-well confinement potentials suggests that J can be varied from 10^{-2} to 10^{-4} eV as the inter-dot distance increases from 5 to 20 nm.[69] Self-assembled dots with vertical inter-dot distance as small as 2 nm can be easily fabricated.[68] With a given physical inter-dot distance, an effective inter-dot distance can be electronically tuned with gate voltages, which turn on and off the exchange interaction. The electron energy spacing ΔE_e of a self-assembled dot is about $10^{-2}-10^{-1}$ eV, depending on the geometry and size of the dot.[70] Therefore, the value of J that satisfies the dual condition lies between 10^{-4} and 10^{-3} eV, which is achievable with vertically stacked self-assembled dots. In conclusion, with J between 10^{-4} and 10^{-3} eV, the error due to hyperfine-coupling induced inhomogeneities in Zeeman energies is smaller than the threshold for error correction, and the qubit leakage to higher orbitals can be effectively prevented.

Second, we consider the effect of the electron-nuclear spin interaction on a single-qubit operation. The single-qubit operation using the Zeeman coupling to an electron spin resonance (ESR) field $(B_{ac} \cos \omega_{ac} t)$ involves the tuning of the ESR field frequency to the electron-spin precession frequency or vice versa. This tuning can be achieved by tuning the ESR field frequency[11] or by tuning the electron g-factor via an applied voltage.[6,8,34,36] The tuning process becomes complicated in the presence of the effective nuclear magnetic field $\mathbf{B}_N$ generated by the electron-nuclear spin interaction, because $\mathbf{B}_N$ affects the electron-spin precession frequency. The effective nuclear magnetic field $\mathbf{B}_N$ fluctuates in space from one qubit to another and evolves in time. The spatial fluctuation of B_N can be compensated by calibrating the gate voltage for each qubit separately. However, the temporal evolution of B_N is difficult to compensate since a gate calibration cannot be done immediately before each operation. The temporal evolution is determined by many competing interactions such as the Zeeman coupling of the nuclear spin to the external magnetic field, the nuclear spin interaction with the electron spin, the nuclear spin dipolar interaction, and the nuclear spin–lattice interaction. Detailed studies of the temporal evolution of $\mathbf{B}_N$ that include these interactions are needed to determine how long a single-qubit gate calibration is valid.

Here, we estimate the upper limit of the temporal change of $\mathbf{B}_N$ for a single-qubit gate calibration to be valid. We assume that a static magnetic field B_0 of the order of 1 T is applied, and that an ESR field of the order of 10^{-3} T is used for the spin rotation.[4,6,8] The precession frequency of the electron spin is given by $\omega_e = g_e \mu_B \sqrt{(B_0 + B_N^{\parallel})^2 + (B_N^{\perp})^2}$, where $B_N^{\parallel}$ and $B_N^{\perp}$ are the $\mathbf{B}_N$ component parallel and perpendicular to B_0, respectively. A single-qubit gate will be calibrated by tuning the frequency of the ESR field ω_{ac} to ω_e. After some time,[71] $B_N^{\parallel}$ and $B_N^{\perp}$ will change by $\Delta B_N^{\parallel}$ and $\Delta B_N^{\perp}$ due to the nuclear spin dynamics, and ω_e will change accordingly. This will lead to detuning of the ESR field. The frequency difference $\omega_{ac} - \omega_e$ is approximately $g_e \mu_B (\Delta B_N^{\parallel} + (B_N^{\perp}/B_0)\Delta B_N^{\perp})$, using the fact that $B_0 \gg B_N$ for unpolarized nuclear spins, where B_N is on the order of 0.01 T. The error due to the detuning in the single-qubit operation is proportional to $(\omega_{ac} - \omega_e)^2/(g_e \mu_B B_{ac})^2$. To ensure that the error is smaller than the threshold value (10^{-4}) given by error correction codes,[66,67] $\Delta B_N^{\parallel}$ and $\Delta B_N^{\perp}$ should be smaller than 10^{-5} and 10^{-3} T, respectively. If $\Delta B_N^{\parallel}$ and $\Delta B_N^{\perp}$ during the time interval between calibration and the termination of a computation are bigger than these upper limits, the single-qubit gate calibration becomes invalid, and thus QC architectures using only exchange interactions should be employed.[72–74] The exchange interaction alone can provide universal quantum gates with a minimal cost of increasing the number of required physical qubits by three times and of increasing the number of gate operations by five to seven times.[73]

V. CONCLUSION

The effect of electron-nuclear spin interactions on qubit operations is investigated here for a qubit represented by the electron spin localized in an InGaAs self-assembled quantum dot. The localized electron wave function is evaluated within the atomistic tight-binding model. The hyperfine splitting induced by the electron-nuclear spin interaction is estimated in the presence of an inhomogeneous environment characterized by random nuclear configurations, dot-size fluctuations, and alloy and interface disorder. Due to the inhomogeneities, the hyperfine splitting fluctuates from dot to dot on the order of 10^{-6}, 10^{-6}, 10^{-7}, and 10^{-9} eV, respectively.

The inhomogeneous hyperfine splitting causes an error in a two-qubit operation due to the inequality of the Zeeman splitting of the two qubits. However, these errors can be made smaller than the quantum error threshold, as long as the exchange energy for the two-qubit operation is larger than 10^{-4} eV. Recent work indicates that an exchange energy of 10^{-4} eV or larger is easily achievable with vertically stacked quantum dots.[69,75,76] At the same time, the large energy spacing between the ground and the excited orbital $(10^{-2}-10^{-1}$ eV) of the quantum dots ensures that the electron qubit stays in the ground orbital while the two-qubit operation is conducted.[70] This result shows that the electron-nuclear spin interaction does not hinder quantum-dot based quantum computer architectures from being scalable even in the presence of inhomogeneous environments causing inhomogeneous hyperfine splittings.

We also estimated the upper limit of the temporal change of the nuclear magnetic field for a single-qubit gate calibration to be valid when an electron resonance field is used for a single-qubit operation. The changes of the nuclear magnetic field parallel and perpendicular to the external static magnetic field should be smaller than 10^{-5} and 10^{-3} T, respectively. When this condition is not met, QC architectures using only exchange interactions should be employed.[72–74] As shown above, the two-qubit operation using the exchange interaction is reliable even in the presence of the inhomogeneous environment of self-assembled quantum dots.

TABLE III. Tight-binding coefficients of the s and s^* basis orbitals for the conduction-band-edge wave functions of bulk InAs and GaAs, and deduced densities of s and s^* orbitals at nuclear sites. The densities $|\phi_s(0)|^2$ and $(\phi_{s^*}|0|^2)$ are in units of 10^{25}cm^{-3}.

Atom	α	β	$|\phi_s(0)|^2$	$|\phi_{s^*}(0)|^2$
In in InAs	0.974	0.228	7.9	2.2
As in InAs	0.872	−0.489	18.4	1.7
Ga in GaAs	0.988	0.157	5.2	1.0
As in GaAs	0.869	−0.576	20.2	1.8

ACKNOWLEDGMENTS

APPENDIX: DENSITY OF AN ATOMIC BASIS ORBITAL AT A NUCLEAR SITE

In principle, a measurement of the Overhauser shift of the electron spin resonance provides the density of the conduction electron at the nuclear site.[78] Although Overhauser shifts for bulk InAs and GaAs have not been measured, the densities of an atomic orbital at a nuclear site for InAs and GaAs can be deduced from the Overhauser shifts measured for bulk InSb.[59] The measured densities for InSb are $9.4 \times 10^{25} \text{ cm}^{-3}$ at In nuclear site and $1.6 \times 10^{26} \text{ cm}^{-3}$ at Sb nuclear site. From the measured densities, Paget *et al.*[79] deduced the densities for InAs and GaAs, using the similarity of the ionicity of InAs and GaAs compared to that of InSb.[80]

$$|\psi(0)|^2_{(\text{In in InAs})} \simeq 9.4 \times 10^{25} \text{ cm}^{-3}, \tag{A1}$$

$$|\psi(0)|^2_{(\text{As in InAs})} \simeq 9.8 \times 10^{25} \text{ cm}^{-3}, \tag{A2}$$

$$|\psi(0)|^2_{(\text{Ga in GaAs})} \simeq 5.8 \times 10^{25} \text{ cm}^{-3}, \tag{A3}$$

$$|\psi(0)|^2_{(\text{As in GaAs})} \simeq 9.8 \times 10^{25} \text{ cm}^{-3}. \tag{A4}$$

The density $|\psi(0)|^2$ for each atom in bulk is related to the tight-binding orbitals $\phi_{s^*}(0)$ and $\phi_s(0)$ as follows:

$$|\psi(0)|^2 = |\alpha\phi_s(0) + \beta\phi_{s^*}(0)|^2, \tag{A5}$$

where α and β are the tight-binding coefficients for the conduction-band edge wave function in bulk. These coefficients are listed in Table III. Determining the unknown values $\phi_s(0)$ and $\phi_{s^*}(0)$ requires one more equation in addition to Eq. (A5). We assume that the ratio $\phi_{s^*}(0)/\phi_s(0)$ is equal to the ratio of the corresponding atomic orbitals. The atomic orbital can be described by a hydrogen-like atomic orbital with an effective nuclear charge.[81,82] The ratios $\phi_{s^*}(0)/\phi_s(0)$ for In, Ga, and As atoms are 0.53, 0.44, and 0.30, respectively. Finally, by inserting the deduced density $|\psi(0)|^2$, the conduction-band edge coefficients α, β, and the orbital ratio $\phi_{s^*}(0)/\phi_s(0)$ into Eq. (A5), the densities of the s and s^*

orbitals are obtained. The resulting densities are listed in Table III.

[1] A. Ekert and R. Jozsa, Rev. Mod. Phys. **68**, 733 (1996).
[2] N. A. Gershenfeld and I. L. Chuang, Science **275**, 350 (1997).
[3] F. Yamaguchi and Y. Yamamoto, Appl. Phys. A: Mater. Sci. Process. **68**, 1 (1999).
[4] B. E. Kane, Nature (London) **393**, 133 (1998).
[5] J. Twamley, Phys. Rev. A **67**, 052318 (2003).
[6] D. Loss and D. P. DiVincenzo, Phys. Rev. A **57**, 120 (1998).
[7] A. Imamoglu, D. D. Awschalom, G. Burkard, D. P. DiVincenzo, D. Loss, M. Sherwin, and A. Small, Phys. Rev. Lett. **83**, 4204 (1999).
[8] R. Vrijen, E. Yablonovitch, K. Wang, H. W. Jiang, A. Balandin, V. Roychowdhury, T. Mor, and D. Divincenzo, Phys. Rev. A **62**, 012306 (2000).
[9] I. L. Chuang, L. M. K. Vandersypen, X. Zhou, D. W. Leung, and S. Lloyd, Nature (London) **393**, 143 (1998).
[10] L. M. K. Vandersypen, M. Steffen, G. Breyta, C. S. Yannoni, R. Cleve, and I. L. Chuang, Phys. Rev. Lett. **85**, 5452 (2000).
[11] L. M. K. Vandersypen, M. Steffen, G. Breyta, C. S. Yannoni, M. H. Sherwood, and I. L. Chuang, Nature (London) **414**, 883 (2001).
[12] S. Gulde, M. Riebe, G. P. T. Lancaster, C. Becher, J. Eschner, H. Haffner, F. Schmidt-Kaler, I. L. Chuang, and R. Blatt, Nature (London) **421**, 48 (2003).
[13] D. P. Divincenzo and P. W. Shor, Phys. Rev. Lett. **77**, 3260 (1996).
[14] A. M. Steane, Nature (London) **399**, 124 (1999).
[15] D. Gottesman and I. L. Chuang, Nature (London) **402**, 390 (1999).
[16] E. Knill, R. Laflamme, and W. H. Zurek, Science **279**, 342 (1998).
[17] X. Hu, R. de Sousa, and S. D. Sarma, Phys. Rev. Lett. **86**, 918 (2001).
[18] T. Ishikawa, S. Kohmoto, and K. Asakawa, Appl. Phys. Lett. **73**, 1712 (1998).
[19] H. Lee, J. A. Johnson, M. Y. He, J. S. Speck, and P. M. Petroff, Appl. Phys. Lett. **78**, 105 (2001).
[20] M. Borgstrom, J. Johansson, L. Samuelson, and W. Seifert, Appl. Phys. Lett. **78**, 1367 (2001).
[21] R. L. Williams, G. C. Aers, P. J. Poole, J. Lefebvre, D. Chithrani, and B. Lamontagne, J. Cryst. Growth **223**, 321 (2001).
[22] R. Songmuang, S. Kiravittaya, and O. G. Schmidt, Appl. Phys. Lett. **82**, 2892 (2003).
[23] S. Watanabe, E. Pelucchi, B. Bwir, M. H. Baier, K. Leifer, and E. Kapon, Appl. Phys. Lett. **84**, 2907 (2004).
[24] D. Chithrani, R. L. Williams, J. Lefebvre, P. J. Poole, and G. C. Aers, Appl. Phys. Lett. **84**, 978 (2004).
[25] I. A. Merkulov, A. L. Efros, and M. Rosen, Phys. Rev. B **65**, 205309 (2002).
[26] S. W. Brown, T. A. Kennedy, D. Gammon, and E. S. Snow, Phys. Rev. B **54**, R17339 (1996).
[27] D. Gammon, S. W. Brown, E. S. Snow, T. A. Kennedy, D. S. Katzer, and D. Park, Science **277**, 85 (1997).
[28] J. K. Kikkawa and D. D. Awschalom, Science **287**, 473 (2000).
[29] G. Salis, D. T. Fuchs, J. M. Kikkawa, D. D. Awschalom, Y. Ohno, and H. Ohno, Phys. Rev. Lett. **86**, 2677 (2001).
[30] A. Imamoglu, E. Knill, L. Tian, and P. Zoller, Phys. Rev. Lett. **91**, 017402 (2003).
[31] M. J. Snelling, G. P. Flinn, A. S. Plaut, R. T. Harley, A. C. Tropper, R. Eccleston, and C. C. Phillips, Phys. Rev. B **44**, 11345 (1991).
[32] M. J. Snelling, E. Blackwood, C. J. McDonagh, R. T. Harley, and C. T. B. Foxon, Phys. Rev. B **45**, 3922 (1992).
[33] A. A. Kiselev, E. L. Ivchenko, and U. Rössler, Phys. Rev. B **58**, 16353 (1998).
[34] Y. Kato, R. C. Myers, D. C. Driscoll, A. C. Gossard, J. Levy, and D. D.

Awschalom, Science **299**, 1201 (2003).

[35]R. de Sousa and S. D. Sarma, Phys. Rev. B **68**, 155330 (2003).

[36]G. Salis, Y. Kato, K. Ensslin, D. C. Driscoll, A. C. Gossard, and D. D. Awschalom, Nature (London) **414**, 619 (2001).

[37]A. V. Khaetskii and Y. V. Nazarov, Phys. Rev. B **64**, 125316 (2001).

[38]S. I. Erlingsson, Y. V. Nazarov, and V. I. Fal'ko, Phys. Rev. B **64**, 195306 (2001).

[39]A. V. Khaetskii, D. Loss, and L. Glazman, Phys. Rev. Lett. **88**, 186802 (2002).

[40]J. Schliemann, A. V. Khaetskii, and D. Loss, Phys. Rev. B **66**, 245303 (2002).

[41]S. I. Erlingsson and Y. V. Nazarov, Phys. Rev. B **66**, 155327 (2002).

[42]R. de Sousa and S. D. Sarma, Phys. Rev. B **67**, 033301 (2003).

[43]R. de Sousa and S. D. Sarma, Phys. Rev. B **68**, 115322 (2003).

[44]A. V. Khaetskii, D. Loss, and L. Glazman, Phys. Rev. B **67**, 195329 (2003).

[45]F. R. Waugh, M. J. Berry, D. J. Mar, R. M. Westervelt, K. L. Campman, and A. C. Gossard, Phys. Rev. Lett. **75**, 705 (1995).

[46]C. Livermore, C. H. Crouch, R. M. Westervelt, K. L. Campman, and A. C. Gossard, Science **274**, 1332 (1996).

[47]B. H. Brandsden and C. J. Joachain, *Physics of Atoms and Molecules* (Longman Scientific & Technical, New York, 1983).

[48]S. L. Richardson, M. L. Cohen, S. G. Louie, and J. R. Chelikowsky, Phys. Rev. B **33**, 1177 (1986).

[49]P. Boguslawsky and I. Gorczyca, Semicond. Sci. Technol. **9**, 2169 (1994).

[50]J.-M. Jancu, R. Scholz, F. Beltram, and F. Bassani, Phys. Rev. B **57**, 6493 (1998).

[51]T. B. Boykin, G. Klimeck, R. C. Bowen, and F. Oyafuso, Phys. Rev. B **66**, 125207 (2002).

[52]J. M. Moison, F. Houzay, F. Barthe, L. Leprince, E. André, and O. Vatel, Appl. Phys. Lett. **64**, 196 (1994).

[53]N. P. Kobayashi, T. R. Ramachandran, P. Chen, and A. Madhukar, Appl. Phys. Lett. **68**, 3299 (1996).

[54]I. Mukahametzhanov, J. Wei, R. Heitz, and A. Madhukar, Appl. Phys. Lett. **75**, 85 (1999).

[55]P. Keating, Phys. Rev. **145**, 637 (1966).

[56]P.-O. Löwdin, J. Chem. Phys. **18**, 365 (1950).

[57]W. A. Harrison, *Elementary Electronic Structure* (World Scientific, New Jersey, 1999).

[58]J. C. Slater and G. F. Koster, Phys. Rev. **94**, 1498 (1954).

[59]M. Gueron, Phys. Rev. **135**, 200 (1964).

[60]D. C. Dixon, K. R. Wald, P. L. McEuen, and M. R. Melloch, Phys. Rev. B **56**, 4743 (1997).

[61]T. Machida, S. Ishizuka, T. Yamazaki, S. Komiyama, K. Muraki, and Y. Hirayama, Phys. Rev. B **65**, 233304 (2002).

[62]F. Patella, M. Fanfoni, F. Arciprete, S. Nufris, E. Placidi, and A. Balzarotti, Appl. Phys. Lett. **78**, 320 (2001).

[63]B. Lita, R. S. Goldman, J. D. Phillips, and P. K. Bhattacharya, Appl. Phys. Lett. **75**, 2797 (1999).

[64]S. J. Xu, H. Wang, Q. Li, M. H. Xie, X. C. Wang, W. J. Fan, and S. L. Feng, Appl. Phys. Lett. **77**, 2130 (2000).

[65]X. Hu and S. D. Sarma, Phys. Rev. A **68**, 052310 (2003).

[66]A. M. Steane, Phys. Rev. A **68**, 042322 (2003).

[67]D. Gottesman, Ph.D. thesis, California Institute of Technology, quant-ph/9705052 (1997).

[68]J. Ibanez, A. Patane, M. Henini, L. Eaves, S. Hernandez, R. Cusco, L. Artus, Y. G. Musikhin, and P. N. Brounkov, Appl. Phys. Lett. **83**, 3069 (2003).

[69]G. Burkard, D. Loss, and D. P. DiVincenzo, Phys. Rev. B **59**, 2070 (1999).

[70]R. Heitz, O. Stier, I. Mukhametzhanov, A. Madhukar, and D. Bimberg, Phys. Rev. B **62**, 11017 (2000).

[71]Here, we are concerned about the change of the effective nuclear magnetic field $\mathbf{B}_N$ during the time period between the gate calibration and the gate operation rather than during the time period for the gate operation. The field $\mathbf{B}_N$ varies on a time scale of 10^{-4} s due to the nuclear dipole-dipole interaction. We do not know exactly how long it takes to calibrate all the gates individually (perhaps minutes or hours). However, the gate calibration time is certainly much longer than 10^{-4} s. In contrast, the gate operation time, which is roughly given by an ESR pulse length 10^{-9} s using the ESR field 10 G, is much shorter than 10^{-4} s.

[72]J. Kempe, D. Bacon, D. A. Lidar, and K. B. Whaley, Phys. Rev. A **63**, 042307 (2001).

[73]J. Kempe and K. B. Whaley, Phys. Rev. A **65**, 052330 (2002).

[74]D. P. DiVincenzo, D. Bacon, J. Kempe, G. Burkard, and K. B. Whaley, Nature (London) **408**, 339 (2000).

[75]M. H. Son, J. H. Oh, D. Y. Jeong, D. Ahn, M. S. Jun, S. W. Hwang, J. E. Oh, and L. W. Engel, Appl. Phys. Lett. **82**, 1230 (2003).

[76]M. Bayer, P. Hawrylak, K. Hinzer, S. Fafard, M. Korkusinski, Z. R. Wasilewski, O. Stern, and A. Forchel, Science **291**, 451 (2001).

[77]G. Klimeck, F. Oyafuso, T. B. Boyking, R. C. Bowen, and P. von Allmen, Computer Modeling in Engineering and Science **3**, 601 (2002).

[78]A. W. Overhauser, Phys. Rev. **92**, 411 (1953).

[79]D. Paget, G. Lampel, B. Sapoval, and V. I. Safarov, Phys. Rev. B **15**, 5780 (1977).

[80]J. C. Phillips, *Bonds and bands in semiconductors* (Academic, New York, 1973).

[81]E. Clementi and D. L. Raimondi, J. Chem. Phys. **38**, 2686 (1963).

[82]E. Clementi, D. L. Raimondi, and W. P. Reinhardt, J. Chem. Phys. **47**, 1300 (1967).